A NOVEL ARTIFICIAL POTENTIAL FIELD APPROACH CONSIDERING ANGULAR ACCELERATION CONSTRAINT

Mingxiao Sun,*,**,***,**** Zhangjie Yuan,* Yongde Zhang,*** Liqiang Zhen,*
Tiantian Luan,*,**,*** Xiaoliang Yuan,**** and Xiaogang Li,****

Abstract

An improved artificial potential field approach (APFA) is proposed for unmanned surface vehicle (USV) in path planning. The proposed approach can effectively avoid easily falling into local minima, also, plan the optimal path. Firstly, a map of the Marine environment is established, and the obstacle is treated with circular expansion. Especially, the expansion coefficient is introduced to ensure the safety of navigation. Secondly, aiming at the local minimum problem, a rotation angle formula satisfying its own maximum rotation angle and angular acceleration constraints is constructed, so that a path to avoid local minimum is planned. Moreover, the local minimum of the complex environment is considered, the virtual repulsive force potential field is constructed to generate virtual repulsive force on USV to avoid local minimum. Numerical simulation results show that the proposed approach can complete path planning under different complex and special environments.

Key Words

Artificial potential field approach (APFA), unmanned surface vehicle (USV), path planning, local minimum

1. Introduction

The unmanned surface vehicle (USV) is an autonomous marine vehicle. The USV has become an indispensable tool in the fields of marine scientific research, resource development, and environmental monitoring [1]. Autonomy is an important feature of USV development and path planning plays a vital role in the development of USV autonomy.

Path planning is related to USV mission execution efficiency and navigation safety. Path planning is mainly divided into two categories: global static path planning with known complete map information and local dynamic path planning with real-time update of some map information. At present, the algorithms of global static path planning mainly include A* algorithm [2], [3], particle swarm optimisation algorithm (PSO) [4]–[6], ant colony algorithm [7], [8], genetic algorithm [9], [10], neural network algorithm [11], [12], and artificial potential field approach (APFA) [13], [14]. The APFA has the advantages of short calculation time, simple principle, and smooth generation path. It is widely used in USV path planning.

The APFA was originally a virtual potential field method constructed by Oussama [15] when he studied the manipulator arm. Wu *et al.* [16] proposed a new lane changing of autonomous vehicles algorithm. Victor *et al.*[17] proposed a new dynamic fractional repulsion force based on the speed of the obstacle. To sum up, although the references improve the practicability of the algorithm to a certain extent, it is easy to fall into the local minimum problem without considering the APFA.

For the local minimum problem, some scholars solve it by merging with other algorithms. For example, Xu *et al.* [18] introduced the decreasing coefficient of potential field resultant force. Zhang *et al.* [19] combined the attraction of target points in the force field with RRT. Lee *et al.* [20] added an adjustment factor to change the repulsion potential field function. Chen *et al.*[21] introduced the collision risk degree to determine the impact distance of obstacles. The literatures solve the traditional local minimum problem of APFA to a certain extent, but do not consider the local minimum problem in complex special environment.

This paper mainly solves the local minimum problem of path planning of surface unmanned craft

* School of Automation, Harbin University of Science and Technology, No. 52 Xuefu Road, Nangang District, Harbin City 150080, Heilongjiang Province, China; e-mail: sunmingxiao@hrbust.edu.cn; {a15582408101,zhangyd1103}@163.com; 2472019567@qq.com; luantiantian@hrbust.edu.cn
** Heilongjiang Provincial Key Laboratory of Complex Intelligent System and Integration, Harbin University of Science and Technology, No. 52 Xuefu Road, Nangang District, Harbin City 150080, Heilongjiang Province, China;
*** Key Laboratory of Advanced Manufacturing and Intelligent Technology, Ministry of Education, Harbin University of Science and Technology, No. 52 Xuefu Road, Nangang District, Harbin City 150080, Heilongjiang Province, China;
**** Wuxi CREG Urban Rail Transit Equipment Co., Ltd., No. 1061, Jiaoshan Road, Xishan Development Zone, Wuxi City 214000, Jiangsu Province, China; e-mail: yuanxiaoliang2022@yeah.net; 372572938@qq.com.
Corresponding author: Yongde Zhang

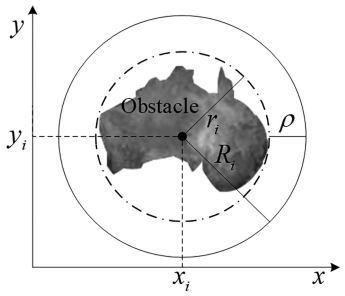

Figure 1. Obstacle model diagram.

by using the traditional artificial potential field method.

2. Problem Description

2.1 Environmental Modelling

At sea level, most obstacles encountered by USV are islands or reefs. The circular expansion method is used to simplify the complexity of modelling, and the expansion coefficient is introduced to avoid the stranding of USV and ensure the safety of USV.

As shown in Fig. 1, the circle enclosed by the dotted line is the envelope circle of the obstacle, the center of the circle is marked as (x_i, y_i), the radius is marked as r_i, and i is the serial number of the obstacle. The expansion coefficient ρ is set as n times of the radius r_i of the obstacle envelope circle (in this paper, $n = 0.48$). The envelope circle with increased expansion coefficient is taken as the restricted navigation zone covering the obstacle, that is, the solid line circle in Fig. 1, and its radius $R_i = r_i + \rho$.

2.2 Artificial Potential Field Approach (APFA)

The core idea of APFA was inspired by natural potential field in physics, the mathematical function of this action mechanism is applied to the environmental model of USV. The initial point position is $q_s = (x_s, y_s)^T$. The target point position is $q_g = (x_g, y_g)^T$. The gravitational potential field $U_a(q)$ is established for q_g. The obstacle position in the map is $q_o = (x_i, y_i)^T, i = 1, 2, \ldots$, and the repulsive potential field $U_r(q)$ is established for the obstacle. USV real-time position $q = (x, y)^T$, so the potential field function $U(q)$ of USV at position q is expressed as:

$$U(q) = U_a(q) + U_r(q) \tag{1}$$

where the equation of gravitational potential field $U_a(q)$ is:

$$U_a(q) = 0.5\mu\rho^2(q, q_g) \tag{2}$$

where μ is the gain coefficient of the gravitational potential field. $\rho(q, q_g)$ is the distance between q and q_g. Since the gravitational direction is USV pointing to the target point, the negative gradient of $U_a(q)$ is obtained and the equation of gravity $F_a(q)$ is obtained as:

$$F_a(q) = -\nabla U_a(q) = -\mu(q - q_g) \tag{3}$$

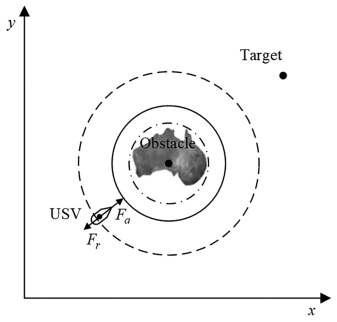

Figure 2. Stress analysis diagram.

The equation of repulsive potential field $U_r(q)$ is:

$$U_r(q) = \begin{cases} \frac{1}{2}\eta\left(\frac{1}{\rho(q,q_o)} - \frac{1}{\rho_0}\right)^2, & \rho(q, q_o) < \rho_0 \\ 0 \qquad\qquad\qquad\quad , & \rho(q, q_o) \geq \rho_0 \end{cases} \tag{4}$$

Then the repulsion force $F_r(q)$ is:

$$F_r(q) = \begin{cases} \eta\left(\frac{1}{\rho(q,q_o)} - \frac{1}{\rho_0}\right)\frac{1}{\rho^2(q,q_o)}, & \rho(q, q_o) < \rho_0 \\ 0 \qquad\qquad\qquad\quad , & \rho(q, q_o) \geq \rho_0 \end{cases} \tag{5}$$

where η represents the gain coefficient of the repulsive potential field. ρ_0 is the influence range of the repulsive potential field. $\rho(q, q_o)$ represents the distance between the current position $q$and the obstacle q_o. The resultant force q at position $F(q)$ is expressed as:

$$F(q) = F_a(q) + F_r(q) \tag{6}$$

USV moves according to the resultant force direction to update the real-time position. The specific update methods are as follows:

$$q(t + 1) = q(t) + \frac{F(q)}{|F(q)|} \cdot v \tag{7}$$

where $q(t + 1)$ is the position at time $t + 1$, $q(t)$ is the position at time t, and v is the navigational speed.

USV moves according to the resultant force direction. If the resultant force is 0, USV cannot move according to the direction of resultant force. USV will fall into a local minimum.

3. Improved Artificial Potential Field Method

3.1 Construct Rotation Angle Equation

In order to solve the local minimum problem, [22] has carried out theoretical analysis and simulation verification on four methods, such as obstacles are wound around, obstacle repulsion is increased, subhead punctuation is automatically added and subhead punctuation is manually added. These methods fall into the local minimum and then break away from the local minimum, which leads to low obstacle avoidance efficiency, poor security, path jitter, and other problems.

As shown in Fig. 2, when gravity and repulsion are collinear and opposite, the USV may fall into the local

minimum if it continues to drive forward. Therefore, at this time, according to the real-time position of USV and obstacle information, the rotation angle equation is constructed to leave the influence range of obstacles, so as the USV gets rid of the local minimum.

When $F_r(q)$ is collinear opposite to $F_a(q)$, the following equation shall be satisfied:

$$F_r(q)/F_a(q) < 0 \tag{8}$$

If the above equation is satisfied, the position is recorded as q_v and the corner equation is constructed:

$$\theta = \left(1 - \frac{\rho\left(q, q_o^{\min}\right) - \rho_0}{\rho_0 - R}\right)\theta_{\max} \tag{9}$$

where θ is the rotation angle, $\theta_{\max}$ is the maximum rotation angle, $\rho(q, q_o^{\min})$ represents the distance between q and the nearest obstacle $q_o^{\min}$ of the USV within the influence range of the repulsive potential field. When the USV is at the edge of the actual range of the obstacle, if (8) is satisfied. $\rho(q, q_o^{\min}) \to R$, then $\theta \to 2\theta_{\max}$, USV rotates its maximum angle twice in a row to avoid obstacles. To avoid path mutation caused by too large rotation angle, the angular acceleration equation is constructed:

$$\theta_{\text{curr}}(t) = \theta_{\text{curr}}(t - \Delta t) + \omega_{\max} \cdot \Delta t \tag{10}$$

where $\theta_{\text{curr}}(t)$ represents the current angle, $\theta_{\text{curr}}(t - \Delta t)$ represents the angle at the previous time, Δt represents the sampling interval, and $\omega_{\max}$ represents the maximum angular acceleration of USV.

In order to ensure navigation safety, when USV is no longer close to obstacles, the USV keeps the current heading unchanged, that is, when the real-time position of USV meets:

$$\rho(q(t), q_o^{\min}) > \rho(q(t-1), q_o^{\min}) \tag{11}$$

where $q(t-1)$ is the position of USV at the previous time. If the position relationship between the USV at this moment and the previous moment satisfies the above formula, it indicates that the USV at this moment is far away from the nearest obstacle and the current course is a safe course. The USV keeps the current course and continues to move forward to ensure navigation safety.

The USV updates the real-time position according to the current angle, that is:

$$q(t+1) = q(t) + v \cdot [\cos(\theta_{\text{curr}}), \sin(\theta_{\text{curr}})]^T \tag{12}$$

3.2 Establishment of Virtual Repulsion Potential Field

When the obstacle environment is complex, as shown in Fig. 3, the USV represented by the dotted line in the figure can get rid of the local minimum problem by using the method described in Section 2.1.

To avoid falling into the local minimum again, the virtual repulsion is added to exert a repulsion on the USV

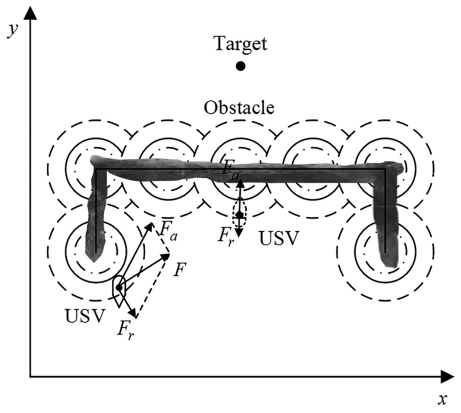

Figure 3. Complex environment diagram.

away from the local minimum. Adding virtual repulsion should satisfy:

$$\rho(q_s, q_j) < \rho(q_s, q_v) \tag{13}$$

where q_j is the position where USV gets rid of the local minimum, $\rho(q_s, q_j)$ represents the distance between q_s and q_j, and $\rho(q_s, q_v)$ represents the distance between q_s and q_v. If the requirements are met, q_v is added to the *v_list* virtual repulsion table to construct the virtual repulsion potential field $U_v(q)$. The equation of $U_v(q)$ is as follows:

$$U_v(q) = \begin{cases} \frac{1}{2}\eta_v \left(\frac{1}{\rho(q,q_v)} - \frac{1}{\rho_v}\right)^2, & \rho(q,q_v) < \rho(q,q_g) \\ 0 \quad , & \rho(q,q_v) \geq \rho(q,q_g) \end{cases} \tag{14}$$

Then the virtual repulsion $F_v(q)$ is:

$$F_v(q) = \begin{cases} \frac{\eta_v}{\rho^2(q,q_v)} \left(\frac{1}{\rho(q,q_v)} - \frac{1}{\rho_v}\right), & \rho(q,q_v) < \rho(q,q_g) \\ 0 \quad , & \rho(q,q_v) \geq \rho(q,q_g) \end{cases} \tag{15}$$

where η_v represents the gain coefficient of $F_v(q)$. ρ_v is the influence range of $F_v(q)$. $\rho(q, q_v)$ represents the distance between q and q_v. After adding the $F_v(q)$, the $F(q)$ at q is expressed as:

$$F(q) = F_a(q) + F_r(q) + F_v(q) \tag{16}$$

4. Algorithm Implementation Process

S1: *Map initialisation:* The model of obstacles in the map, q_s and q_g are established.

S2: *Algorithm parameter initialisation:* μ and η are determined.

S3: Whether the real-time position q reaches q_g needs to be judged. If so, the process of path planning is ended. Otherwise, it carries out S3.1.

S3.1: The $F_a(q)$ and $F_r(q)$ on the current position are calculated according to (3) and (5).

S3.2: According to (8), it is judged whether $F_a(q)$ and $F_r(q)$ of the position q are collinear and opposite. If so, the position is recorded as q_v, and it is executed as S4. Otherwise, S3.3 is executed.

Table 1
Algorithm Parameters

Parameter	Symbol	Value	Unit
Maximum angle	$\theta_{\max}$	0.550	rad
Maximum angular acceleration	$\omega_{\max}$	0.088	rad/s^2
Speed	v	19.400	kn
Gain coefficient of the gravitation	u	9.000	–
Gain coefficient of the repulsion	η	0.300	–

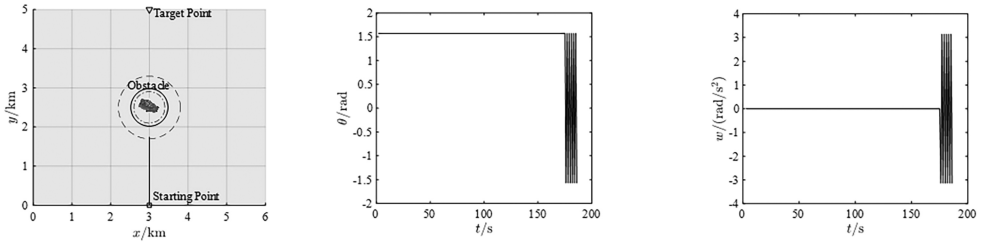

(a) (b) (c)

Figure 4. Map 1: Simulation results of traditional artificial potential field method: (a) route plan diagram; (b) angle change diagram; and (c) angular acceleration change diagram.

S3.3: The *v_list* is judged whether to be empty. If so, $F(q)$ is calculated by (6). Otherwise, $F_v(q)$ and $F(q)$ are calculated by (15) and (16). q is updated by (7) and returns S3.

S4: The USV continues to approach the obstacle is judged using (11). If so, θ_{curr} according to (9) and (10) is calculated. q is updated using (12). If not, USV maintains current course until the USV leaves the range of influence of the nearest obstacle and S5 is returned.

S5: The virtual repulsion potential field is judged according to (13). If so, the virtual repulsive potential field is constructed by adding q_v, then it returns to S3. If not, it returns to S3.

5. Simulation Verification

In order to verify the improved algorithm, two maps are constructed for simulation. The two maps contain a single obstacle and a U-shaped obstacle. The values of algorithm parameters are shown in Table 1.

5.1 Simulation of Local Minimum Problem of Single Obstacle

The improved algorithm, wounding around obstacles algorithm [22], and unimproved algorithm in this paper are used to carry out path planning in Map 1(with a scale of 6×5 km). As shown in Figs. 4–6, the q_s is (3,0), the q_g is (3,5), and the center of the obstacle is set at (3,2.5). The path planned by the traditional APFA is shown in Fig. 4(a), it falls into local minimum at (3, 1.7). The angle change is shown in Fig. 4(b), it falls into local minimum at 175 s. Then USV jumps between $1.571rad$ and $-1.571rad$at $175s - 185s$. Similarly, the angular acceleration jumps between $3.142rad/s^2$ and $-3.142rad/s^2$ as shown in Fig. 4(c). If the algorithm is directly applied, USV will fall into local minimum, which is easy to cause danger.

The results of the obstacles are wound around algorithm are shown in Fig. 5. In Fig. 5(a), compared with the traditional APFA in Fig. 4(a), the USV reaches the local minimum at 175 s in the compared algorithm. After three oscillations, the USV looked for the nearest point at the edge of the obstacle potential field at 179 s. Therefore, the USV angle is abrupt, and then it moves around the obstacle potential field and finally reaches the target point. The angular variation of USV is shown in Fig. 5(b), with dramatic angular changes in many places. The angular acceleration of USV is shown in Fig. 5(c), and the angular acceleration change is not smooth enough to be applied practically.

The path planned by the improved APFA is shown in Fig. 6(a), the local minimum is successfully avoided. The change of angle is shown in Fig. 7(b). At 175 s, the USV falls into a local minimum. The attraction and repulsion are collinear and opposite. The rotation angle is calculated according to (9). The update angle is calculated by (10). The obtained angle changes smoothly and the path is smooth. The change of angular acceleration is shown in Fig. 7(c) and does not exceed $0.088rad/s^2$.

5.2 Simulation of Local Minimum Problem of U-shaped Obstacle

The improved algorithm, wounding around obstacles algorithm [22], and unimproved algorithm in this paper

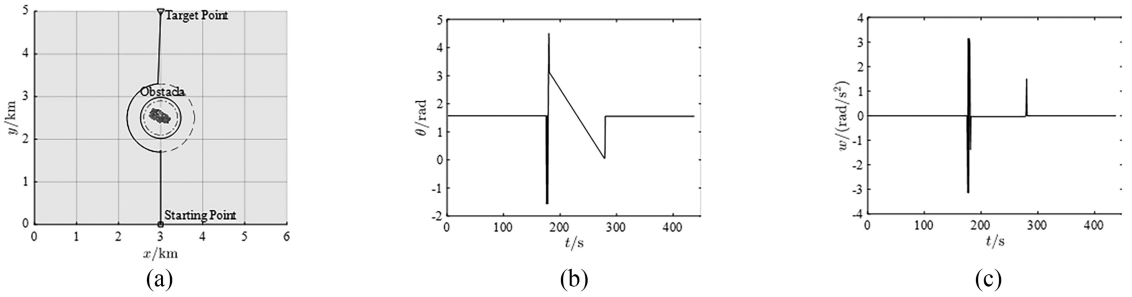

(a) (b) (c)

Figure 5. Map 1: Simulation results of wounding around obstacles algorithm: (a) route plan diagram; (b) angle change diagram; and (c) angular acceleration change diagram.

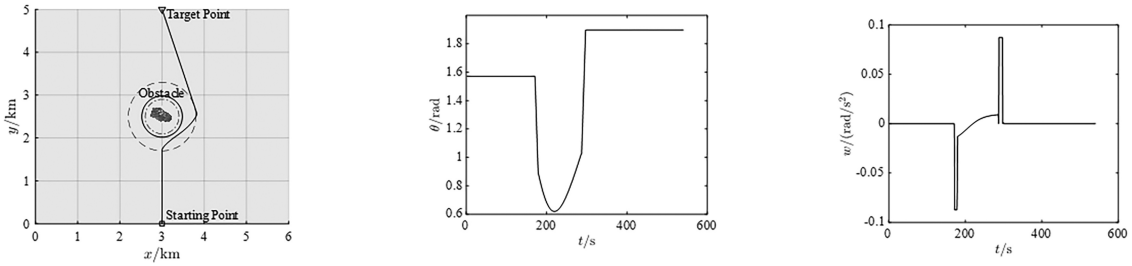

(a) (b) (c)

Figure 6. Map 1: Simulation results of improved artificial potential field method: (a) route plan diagram; (b) angle change diagram; and (c) angular acceleration change diagram.

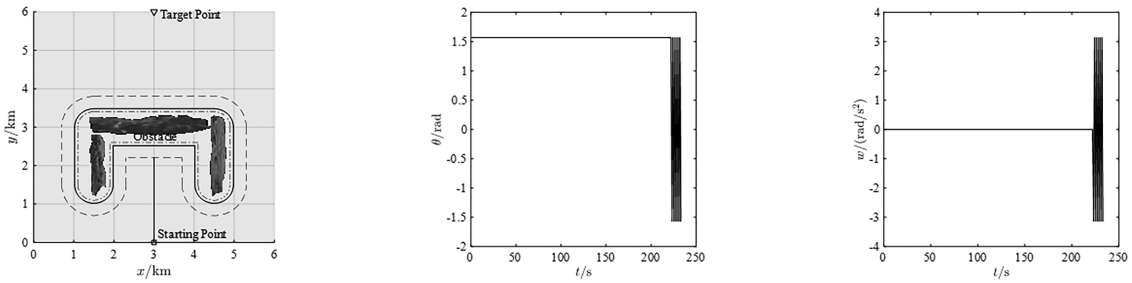

(a) (b) (c)

Figure 7. Map 2: Simulation results of traditional artificial potential field method: (a) route plan diagram; (b) angle change diagram; and (c) angular acceleration change diagram.

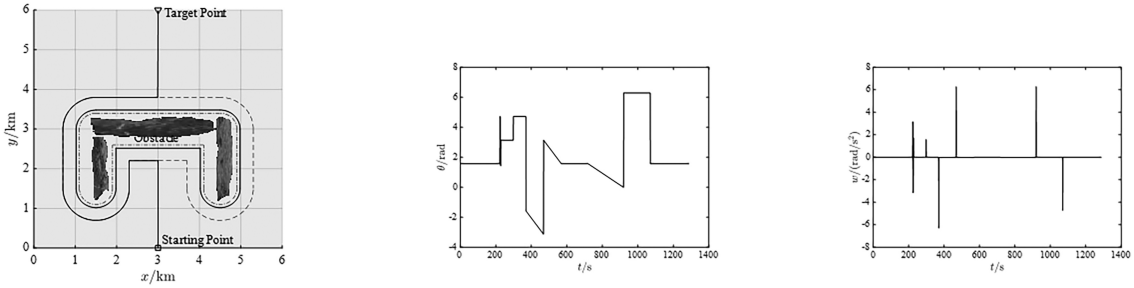

(a) (b) (c)

Figure 8. Map 2: Simulation results of wounding around obstacles algorithm: (a) route plan diagram; (b) angle change diagram; and (c) angular acceleration change diagram.

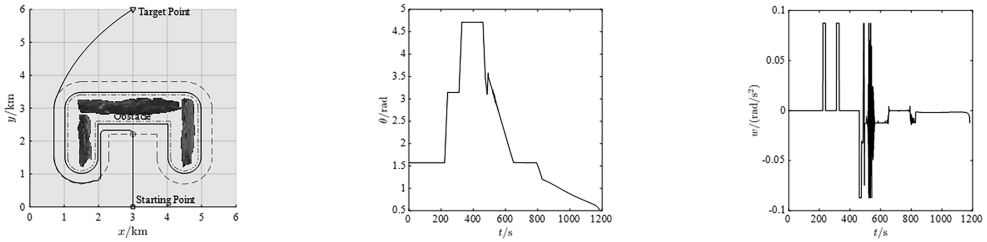

(a) (b) (c)

Figure 9. Map 2: Simulation results of improved artificial potential field method: (a) route plan diagram; (b) angle change diagram; and (c) angular acceleration change diagram.

are used to carry out path planning in Map 2 (with a scale of 6×6 km). As shown in Figs. 7–9, the q_s is (3,0) and the q_g is (3,6), U-shaped obstacle means that the obstacles are arranged in a U-shape. The model is established as shown in Figs. 7–9(a). The path planned by the traditional APFA is shown in Fig. 7(a), which falls into a local minimum at (3, 2.21). The changes of angle and angular acceleration are shown in Fig. 7(b) and 7(c), which are similar with Fig. 4(b) and 4(c). At 222 s, USV falls into a local minimum, at $t = 222 - 232s$, angle jumps and oscillates repeatedly.

The results of the wounding around obstacles algorithm are shown in Fig. 8. In Fig. 8(a), compared with the traditional APFA in Fig. 7(a), the USV reaches the local minimum at 221 s in the compared algorithm. After three oscillations, the USV looked for the nearest point at the edge of the obstacle potential field at 225 s. Therefore, the USV angle is abrupt, and then it moves around the obstacle potential field and finally reaches the target point. The angular variation of USV is shown in Fig. 8(b), with dramatic angular changes in many places. The angular acceleration of USV is shown in Fig. 8(c), and the angular acceleration change is not smooth enough to be applied practically.

The path planned by the improved APFA is shown in Fig. 9(a), which is at (3, 2.21), that is, the collinear opposite position of gravity and repulsion. The rotation angle equation is used to turn, USV avoids the local minimum and reach the target point smoothly. The angle change is shown in Fig. 9(b). The virtual repulsion table is added to the local minimum to increase the virtual repulsion away from the local minimum. The change of angular acceleration is shown in Fig. 9(c). The overall trend does not exceed the maximum angular acceleration limit, because the environment is complex and there are many abrupt changes in angular acceleration.

Conclusion

Local minimum is an inherent problem in traditional artificial potential field method for path planning. In this paper, the improved algorithm is proved by simulation and the results show that in the collinear opposite position of gravity and repulsion, the rotation angle equation between the obstacle position and USV position is constructed. The local minimum can be avoided successfully. In the complex and special environment, the virtual repulsive potential field is established to keep USV away from the local minimum and to avoid USV falling back into the local minimum.

Acknowledgement

This research was funded by the National Science Foundation for Young Scientists of China, grant number 62103120, 51909049, the National Science Foundation for Heilongjiang Province, grant number LH2021F033, Heilongjiang Postdoctoral Grant, grant number LBH-Z22195, LBH-Z22197, and University Nursing Program for Young Scholars with Creative Talents in Heilongjiang Province, grant number UNPYSCT-2020190.

References

[1] Y. Wu, X.C. Su, J.P. Cui, and G. Yang, Coordinated path planning of USV & AUV for an underwater target, *Control and Decision*, *36*, 2021, 825–834.

[2] J. Ji, Z. Ma, J. He, Y. Xu, and Z. Liu, Research on risk evaluation and dynamic escape path planning algorithm based on real-time spread of ship comprehensive fire, *Journal of Marine Science and Engineering*, *8*(8), 2020, 1–21.

[3] Y. Sing, S. Sharma, R. Sutton, and D. Hatton, A constrained A* approach toward optimal path planning for an unmanned surface vehicle in a maritime environment containing dynamic obstacles and ocean currents, *Ocean Engineering*, *169*, 2018, 187–201.

[4] N. Geng, X.Y. Sun, and D.W. Gong, Solving robot path planning in an environment with terrains based on interval multi-objective PSO, *International Journal of Robotics and Automation*, *31*(02), 2016, 100–110.

[5] X. Guo, M. Ji, Z. Zhao, D. Wen, and W. Zhang, Global path planning and multi-objective path control for unmanned surface vehicle based on modified particle swarm optimization (PSO) algorithm, *Ocean Engineering*, *216*, 2020, 1–16.

[6] W. Gan, D. Zhu, and S. Yang, A speed jumping-free tracking controller with trajectory planner for unmanned underwater vehicle, *International Journal of Robotics and Automation*, *35*(05), 2020, 339–346.

[7] J. Li, B. Xu, Y. Yang, and H. Wu, Three-phase qubits-based quantum ant colony optimization algorithm for path planning of automated guided vehicles, *International Journal of Robotics and Automation*, *34*(02), 2019, 156–163.

[8] C. Lin, H. Wang, J. Yuan, and M. Fu, An online path planning method based on hybrid quantum ant colony optimization for AUV, *International Journal of Robotics and Automation*, *33*(04), 2018, 435–444.

[9] L. Wang and C. Luo, A hybrid genetic tabu search algorithm for mobile robot to solve AS/RS path planning, *International Journal of Robotics and Automation*, *33*(02), 2018, 161–168.

[10] Y. Liu, M. Cong, H. Dong, D. Liu, and Y. Du, Time-optimal motion planning for robot manipulators based on elitist genetic

algorithm, *International Journal of Robotics and Automation*, *32*(04), 2017, 396–405.
[11] T. Vodopivec and B. Ster, Selective topological approach to mobile robot navigation with recurrent neural networks, *International Journal of Robotics and Automation*, *30*(05), 2015, 441–446.
[12] S. Sadati, K. Alipour, and M. Behroozi, A combination of neural network and Ritz method for robust motion planning of mobile robots along calculated modular paths, *International Journal of Robotics and Automation*, *23*(03), 2008, 187–198.
[13] J. Wang, X. Lin, H. Zhang, G. Lu, Q. Pan, and H. Li, Path planning of manipulator using potential field combined with sphere tree model, *International Journal of Robotics and Automation*, *35*(02), 2020, 148–161.
[14] M. Sun, Z. Yuan, T. Luan, X. Yuan, and X. Li, USV compliant obstacle avoidance based on dynamic two ship domains, *Ocean Engineering*, 262, 2022, 1–18.
[15] K. Oussama, Real-time obstacle avoidance for manipulators and mobile robots, *The International Journal of Robotics Research*, *5*, 1986, 90–98.
[16] P. Wu, F. Gao, and K. Li, Humanlike decision and motion planning for expressway lane changing based on artificial potential field, *IEEE Access*, *10*, 2022, 4359–5373.
[17] S. Victor, K. Ruiz, P. Melchior, and C. Serge, Dynamical repulsive fractional potential fields in 3D environment, *Fractional Calculus and Applied Analysis*, *25*, 2022, 321–345.
[18] H. Xu, M. Hinostroza, and C. Soares, Modified vector field path-following control system for an underactuated autonomous surface ship model in the presence of static obstacles, *Journal of Marine Science and Engineering*, *9*, 2021, 1–20.
[19] Z. Zhang, D. Wu, J. Gu, and K. Zhu, A path-planning strategy for unmanned surface vehicles based on an adaptive hybrid dynamic stepsize and target attractive force-RRT algorithm, *Journal of Marine Science and Engineering*, *7*, 2019, 1–14.
[20] M. Lee, C. Nieh, H. Kuo, and J. Huang, A collision avoidance method for multi-ship encounter situations, *Journal of Marine Science and Technology*, *25*, 2020, 925–942.
[21] T. Chen, Y. Huang, and C. Li, Cluster path planning based on double potential fields, *Control Theory & Applications*, *38*, 2021, 90–102.
[22] H. Gao, Z. Lyu, B. Wang, K. Xia, L. Mao, X. Wang, and B. Li, Research on local minima of artificial potential field method, *Machinery & Electronics*, *38*(12), 2020, 24–48.

Biographies

Mingxiao Sun is currently an Associate Professor with Harbin University of Science and Technology. His research interests include ship motion control and robot.

Zhangjie Yuan is currently pursuing the undergraduation degree with Harbin University of Science and Technology. His research interests include path planning and trajectory tracking of ship.

Yongde Zhang is currently a Professor with Harbin University of Science and Technology. His research interests include ship motion control and robot.

Liqiang Zhen is currently pursuing the undergraduation degree with Harbin University of Science and Technology. His research interests include ship motion control and robot.

Tiantian Luan is currently an Associate Professor with Harbin University of Science and Technology. Her research interests include control science and engineering, robot, and decision support system.

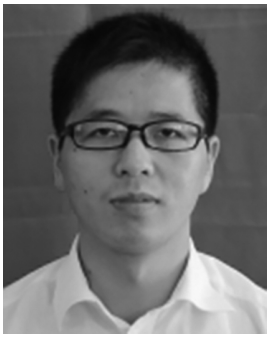

Xiaoliang Yuan is a Senior Engineer with Wuxi CREG Urban Rail Transit Equipment Co., Ltd., Wuxi, China. His research interests include ship motion control and robot.

Xiaogang Li is a Senior Engineer with Wuxi CREG Urban Rail Transit Equipment Co., Ltd., Wuxi, China. His research interests include ship motion control and robot.